INTERFACIAL FORCE FIELD CHARACTERIZATION OF A CONSTRAINED VAPOR BUBBLE THERMOSYPHON USING IAI

Sunando DasGupta, Joel L. Plawsky and Peter C. Wayner, Jr.
The Isermann Department of Chemical Engineering
Rensselaer Polytechnic Institute,
Troy, NY 12180-3590

ABSTRACT

The isothermal profiles of the extended meniscus in a quartz cuvette were measured in a gravitational field using IAI (image analyzing interferometer) which is based on computer enhanced video microscopy of the naturally occurring interference fringes. The experimental results for heptane and pentane menisci were analyzed using the extended Young-Laplace Equation. These isothermal results characterized the interfacial force field *in-situ* at the start of the heat transfer experiments by quantifying the dispersion constant for the specific liquid-solid system. The experimentally obtained values of the disjoining pressures and the dispersion constants are compared to that predicted from the DLP theory and good agreements are obtained. The measurements are critical to the subsequent non-isothermal experiments because one of the major variables in the heat sink capability of the CVBT is the dispersion constant. In all previous studies of micro heat pipes the value of the dispersion constant has been "guesstimated". The major advantages of the current glass cell is the ability to view the extended meniscus at all times. Experimentally, we find that the extended Young-Laplace Equation is an excellent model for the force field at the solid-liquid-vapor interfaces.

INTRODUCTION

When the gravitational body force is essentially removed, the shape of a constrained liquid volume with a free interface changes dramatically to reflect the new force field. The resulting equilibrium shape under microgravity conditions depends on the intermolecular force field which changes rapidly in the vicinity of the liquid-vapor and liquid-solid interfaces. Under non-equilibrium conditions, microgravity fluid dynamics and change of phase heat transfer are a function of further changes in the shape of the fluid volume from its equilibrium shape. Therefore, in small systems, the shape dependent interfacial intermolecular force field can be used to control fluid flow and heat transfer [1, 2]. The initial equilibrium liquid film shape is controlled by fixing the container shape, the liquid and solid substrate surface properties, and the volume of the liquid.

In particular, we are concerned with the experimental study of the generic constrained vapor bubble thermosyphon (CVBT) system presented in Fig. 1. For a completely wetting system, the liquid will coat all the walls of the chamber. For a finite contact angle system, some of the walls will have only a small amount of adsorbed vapor which changes the surface properties of the solid-vapor surface. Liquid will fill a portion of the corners in both cases. If temperature at End (2) is higher than End (1), because of an external heat source and sink, energy flows from End (2) to End (1) by conduction in the walls and by an evaporation, vapor flow and condensation mechanism. The condensate flows from End (1) to End (2) because of the intermolecular force field which is a function of the film profile. A CVBT with a very small cross section has been called a micro heat pipe.

There is a "pressure jump" at the liquid-vapor interface, due to the anisotropic stress tensor near interfaces. For many years, the classical Young-Laplace equation of capillarity has been successfully used to describe the pressure jump at a curved liquid-vapor interface [3, 1, 4, 5, 6, 7, 8, 9]. An example of its use to describe the fluid dynamics in a micro heat pipe is given in a publication by Wu and Peterson [10]. In this case, the pressure jump is a function of the liquid-vapor surface tension and the interfacial radius of curvature. Recently Khrustalev and Faghri [11] and Swanson and Peterson [12] have used this type of model to analyze a micro heat pipe. Swanson and Herdt [13] have used the three dimensional augmented Young-laplace equation to develop a mathematical model describing the evaporating meniscus in a capillary tube. However, near the liquid-solid interface, additional changes in the stress field within the liquid occur because of changes in the intermolecular force field due to solid molecules replacing liquid molecules. These long range van der Waals forces have been found to be extremely important in that they lead to the concept of an extended evaporating meniscus [1, 2]. In a completely wetting system, a thin adsorbed film extends for a long distance beyond the classical equilibrium meniscus [14]. The thin film controls the important processes of spreading and wetting. It forms a thin liquid bridge between the "classical menisci" formed in the corners of the chamber presented in Fig. 1. Herein, we present the initial experimental results of a study of the three dimensional extended meniscus in a configuration of general importance to the microgravity environment : the constrained vapor bubble thermosyphon.

The effects of both the liquid-vapor and liquid-solid interfaces on the effective pressure jump at the liquid-vapor interface of the extended two dimensional meniscus have been modeled using the following augmented Young-Laplace equation. Here P_l is the liquid pressure, P_v is the vapor pressure, $\bar{A}$ is the Hamaker constant (negative for a completely wetting liquid), B is the retarded dispersion constant for thicker films, $\delta(x)$ is the film thickness, K is the curvature and σ is the surface tension. The first term on the right hand side of Eq. (1) is called the disjoining pressure, Π, and it represents the change in the body force on the liquid due to the long range van der Waals forces between the liquid and solid over a narrow range of thicknesses.

$$P_l - P_v = \frac{B}{\delta^n} - \sigma K$$

(1)

$$\frac{B}{\delta^n} = \frac{B}{\delta^4} = -\Pi \quad \delta \geq 40nm \quad ; \quad \frac{B}{\delta^n} = \frac{\bar{A}}{\delta^3} = -\Pi \quad \delta \leq 20nm$$

According to Eq. (1), the effective pressure in the liquid is reduced below that in the vapor by both capillarity and disjoining pressure in a completely wetting system. This leads to a reduction in the vapor pressure. However, the vapor pressure reduction can be offset by a temperature increase to obtain the vapor bubble thermosyphon presented in Fig. 1. The chemical potential field is a function of the temperature and the effective liquid pressure which is a function of the shape of the liquid film. Therefore, the process is understood by measuring the temperature field and the liquid film shape.

THEORY

The augmented Young-Laplace equation can be written for a point in the thicker portion of the meniscus, where the disjoining pressure effects are negligible and for another point where both effects are present. For the isothermal non-evaporating (Q=0) cases considered here the liquid pressure will remain the same, irrespective of the position.

$$\sigma K - \frac{B}{\delta^4} = \sigma K_\infty \quad , \quad Q = 0$$

(2)

We note that the curvature at the thicker portion of the meniscus (K_∞) is nearly constant [15]. In Eq. (2), the curvature at the liquid-vapor interface (K) can be expressed in the following form.

$$K = \frac{\frac{d^2\delta}{dx^2}}{[\,1 + (\frac{d\delta}{dx})^2\,]^{3/2}}$$

(3)

Using a simplified form of curvature, which is valid only if the square of the slope is small compared to one, Eq. (2) can be written in the following way.

$$\sigma \frac{d^2\delta}{dx^2} - \frac{B}{\delta^4} = \sigma K_\infty$$

(4)

For the isothermal experiments reported in this study the value of the maximum slope is 0.15 and hence using the simplified form of curvature is justified. The following variables are introduced next to modify Eq. (4) to obtain Eq. (6).

$$\eta = \frac{\delta}{\delta_0} \qquad Z = x\,(\frac{K_\infty}{\delta_0})^{1/2}$$

(5)

$$\frac{d^2\eta}{dZ^2} + (\frac{-B}{\sigma K_\infty \delta_0^4})\frac{1}{\eta^4} = 1$$

(6)

Eqs 2 - 6 are valid for an equilibrium situation with no evaporation or condensation. A dimensionless variable, α, is defined next.

$$\alpha^4 = \frac{-B}{\sigma K_\infty \delta_0^4}$$

(7)

Eq. (6) can now be written as

$$\frac{d^2\eta}{dZ^2} = 1 - \frac{\alpha^4}{\eta^4} \tag{8}$$

For the equilibrium case, Q=0 and α=1. Any values of α other than unity will signify deviation from the equilibrium situation. The experimental section of the paper and the subsequent discussion will present two experimental cases, which were very close to equilibrium. The results will demonstrate the utility of the model and the evaluation of the values of α. After multiplying both sides of Eq. (8) by $2d\eta/dZ$ and integrating (C_1 is the constant of integration),

$$\left(\frac{d\eta}{dZ}\right)^2 = 2\eta + \frac{2}{3}\frac{\alpha^4}{\eta^3} + C_1 \tag{9}$$

The boundary condition used for the completely wetting case is

$$For \quad \eta = \alpha \quad \frac{d^2\eta}{dZ^2} = 0 = \frac{d\eta}{dZ} \tag{10}$$

We note that this can be viewed as an artificial boundary condition for a non-equilibrium system for which $\alpha > 1$. The utility of the extended model is demonstrated below.

Using the boundary condition, the slope of the meniscus can be expressed as

$$\frac{d\delta}{dx} = - (K_\infty \delta_0)^{1/2} \sqrt{2\eta + \frac{2}{3}\frac{\alpha^4}{\eta^3} - \frac{8}{3}\alpha} \tag{11}$$

Hence if the curvature at the thicker end of the meniscus, K_∞, along with B, δ_0 and σ are known, the slope of the meniscus can be directly calculated as a function of the film thickness, using only the augmented Young-Laplace equation. The minus sign in Eq. (11) is indicative of the fact that for the reference frame selected, the meniscus slope should always be negative (film thickness decreases as distance increases).

Herein we compare the slope of the meniscus obtained by numerical analysis of the experimental data for a system with unknown values of Hamaker constant (or dispersion constant, depending on the adsorbed film thickness) and the slope predicted by the augmented Young-Laplace equation (Eq. 11). The slope predicted by Eq. (11) is a function of α and the α corresponding to the closest match between these two slopes is selected to determine the value of the dispersion constant for the CVBT, in situ, for our isothermal experiments, as will be apparent in the next sections. Finally we compare the experimentally obtained values of the dispersion constants and the disjoining pressures with the predictions from the DLP theory for our experimental system.

EXPERIMENTAL

A schematic diagram of the cell and the experimental set up is shown in Fig. 2. The cell was essentially a small cuvette, made of quartz to facilitate optical observation and measurement of the liquid meniscus. The prototype cell was square (3mm x 3mm inside) in cross section, as is the case with the actual CVBT. The actual CVBT being made is slightly more complicated to facilitate the cleaning (it has a vacuum port, a pure test liquid feed port) and it is made of a special high refractive index glass to enhance the contrast for optical measurements. The present study was conducted as a precursor to the non-isothermal CVBT experiments, mainly to develop the method for accurately measuring the liquid film thickness profile and to estimate the dispersion constant, in situ, at the start of the experiment. The isothermal results characterize the interfacial force field and the information are critical to the operation and the heat sink capability of the CVBT.

The film thickness profile at the corners of the experimental cell was measured using IAI - image analyzing interferometry. Interference phenomena were used to determine the profile of the capillary meniscus in the thickness range $\delta \geq 0.1\mu$m. A detailed description of the IAI techniques and hardware were presented in [15,16]. The cell was partially filled up with the liquid and placed on the microscope stage. The whole assembly was tilted with respect to the horizontal at two different angles in the two settings used in this study. The system was left to equilibrate with the surroundings for 3 hours before taking any data. An optical interference pattern representing the thickness profile was readily observed (Fig. 3). The pictures of the interference patterns formed at the corners of the cell at two specific points (A and B, as shown in Fig. 2) for each angle setting were captured in the image processor. From each image a plot of the pixel grey value versus distance was extracted. The grey value at each pixel was a measure of the reflectivity. As is evident from Fig. 3, the reflectivity underwent a cyclic change with

increase in film thickness. The computer program scanned the peaks and valleys and filtered the noise from the real peaks/valleys. It then interpolated peak/valley envelopes and by analyzing the relative reflectivity of any pixel with respect to these (dark and light pixel envelopes), determined a film thickness at every pixel [16]. The fact that the extended capillary meniscus merged smoothly to an adsorbed flat film was utilized to estimate the adsorbed film thickness from the grey value data and the peak/valley envelopes. The estimated error in measuring the adsorbed film thickness was ±0.5nm-1.0nm for the thickness range studied herein.

Figure 4 is an example of the measured film thickness profiles with heptane as the test liquid. The picture was for a specific angle. In an isothermal system of spreading liquid on an inclined solid substrate the curvature should remain constant in the region where dispersion forces can be neglected. So the film profile in this range approximated a parabola and a plot of $\delta^{1/2}$ vs x was a straight line. As can be seen form Fig. 4, $\delta^{1/2}$ vs x was nearly a straight line in all the cases, showing the proximity of the cases to isothermality. On the other hand it is clear that the thickness profile at point B was steeper than in point A as a result of higher hydrostatic pressures and subsequent higher curvatures. We also observed that an increase in angle resulted in an increase in the film curvature. Plotting $\delta^{1/2}$ vs x, therefore, clearly illustrates the sensitivity of the film thickness shape to externally imposed conditions. This will not be obvious from a plot of δ versus x. Next we address the significance of the film thickness profile measurements.

RESULTS AND DISCUSSION

Figure 5 is a representative picture of the close match between the experimental slope and the slope obtained by the solution of the augmented Young-Laplace equation. The triangles represent the slope at every tenth point obtained by data analysis, whereas the solid line represents the solution of the augmented Young-Laplace equation for the specific value of α. Table 1 summarizes the results for pentane in the small cell inclined at two different angles. Similar results were also obtained for heptane. The values of the dispersion constant for the solid-liquid-vapor system are presented in Table 1. They are calculated from the known values of α corresponding to the minimum error. The values of B for each liquid are reasonably close to each other. We also calculated the dispersion force and the values of B from the DLP theory for quartz-pentane-vapor and quartz-heptane-vapor systems. To calculate the dispersion force from the DLP theory, the same methodology as described in [8, 17] was used. The dielectric functions of the liquids and quartz are obtained from spectroscopic optical data as described by [18]. The results are presented in Table 2 and in Fig. 6. Figure 6 is a plot of the disjoining pressure as a function of the film thickness for heptane wetting on quartz. The solid line is from DLP theory [19], whereas the symbols are from the experiments. Since the dispersion forces for the two alkanes on quartz, as predicted by the DLP theory, are about the same, the experimental data for the pentane-quartz-vapor system are also plotted on the same graph. Both Table 2 and Fig. 6 clearly demonstrate that our experimentally obtained values of B and the disjoining pressures are very close to that predicted from the exact DLP theory.

Table 1 : Selected characteristics of pentane meniscus

	Angle of Inclination = 5.67°				Angle of Inclination = 9.92°			
	δ_0 (nm)	$K_\infty \times 10^{-3}$ (m^{-1})	α	B (J m)	δ_0 (nm)	$K_\infty \times 10^{-3}$ (m^{-1})	α	B (J m)
Point A	22.0	2.512	1.12	1.43×10^{-29}	19.0	3.044	1.04	0.72×10^{-29}
Point B	20.0	3.147	1.04	0.91×10^{-29}	20.0	4.186	1.12	1.63×10^{-29}

Table 2 : Experimental and theoretically calculated values of B(δ) for pentane and heptane on quartz

	n-pentane				n-heptane		
Angle (°)	δ_0 (nm)	B_{expt} (Jm)	B_{DLP} (Jm)	Angle (°)	δ_0 (nm)	B_{expt} (Jm)	B_{DLP} (Jm)
5.67	22.0	1.43×10^{-29}	1.65×10^{-29}	6.24	24.0	2.60×10^{-29}	1.76×10^{-29}
	20.0	0.91×10^{-29}	1.57×10^{-29}		23.0	1.57×10^{-29}	1.73×10^{-29}
9.92	19.0	0.72×10^{-29}	1.53×10^{-29}	9.92	23.0	2.41×10^{-29}	1.73×10^{-29}
	20.0	1.63×10^{-29}	1.57×10^{-29}		22.0	2.71×10^{-29}	1.69×10^{-29}

Similar results were obtained by Gee [17] from adsorption studies of n-alkanes on quartz for high disjoining pressure regimes ($\delta \leq 40\text{Å}$) and by Blake [20], who measured the disjoining pressure as a function of film thickness for n-octane and

n-decane on α-alumina. Blake's techniques demonstrated that Lifshitz theory correctly predicts the results in the low disjoining pressure regimes (δ was between 250Å and 800Å), whereas our present study is concerned with adsorbed film thicknesses of about 200Å. For completeness, we also note that recent studies [21, 22] indicate some limitations of the DLP theory in predicting the interactions in very thin liquid films (below 20Å) and suggest that structural effects are present in some adsorbed films at room temperature, provided the substrates are smooth and homogeneous.

The most important point of the present study is that the dispersion constants for a CVBT (micro heat pipe) system were evaluated in situ at the start of the experiments. This is a definite improvement over previous studies of micro heat pipes where little attention was given to the values of dispersion constants. These constants characterize the interfacial force field and are profoundly important in the basic understanding of the operation and performance of a micro heat pipe. For example, it has been shown that the contact line region in an extended evaporating meniscus, where the intermolecular force effects are important, plays a critical role in the overall heat transfer and liquid flow [1, 14, 12, 23, 24]. Hence our isothermal measurements are critical to the subsequent non-isothermal experiments.

CONCLUSIONS

1. The use of an IAI in conjunction with a CVBT in a gravitational field under isothermal conditions was demonstrated.
2. Procedures to measure the dispersion constant in-situ for the vapor-liquid-solid system were developed.
3. Good agreement between theoretical and experimental values of the dispersion constant was obtained.

ACKNOWLEDGEMENTS

REFERENCES

1. Potash, M., Jr. and Wayner, P.C., Jr., Int. J. Heat Mass Transfer, 15 (1972) 1851-1863.
2. Wayner, P.C., Jr., Kao, Y.K., and LaCroix, L.V., Int. J. Heat Mass Transfer, 19 (1976) 487-492.
3. Derjaguin and Kussakov, Acta Physicochim URSS, 10 (1939) 25.
4. Derjaguin, B.V., and Churaev, N.V., Colloid J. USSR, 38 (1976) 438-448.
5. Teletzke, G. F., Scriven, L. E., and Davis, H. T., Chem. Eng. Comm., 55 (1987) 41-81.
6. Renk, F., Wayner, P.C., Jr., and Homsy, G.M., J. of Colloid and Interface Sci., 67 (1978) 408-414.
7. Moosman, S. and Homsy, S.M., J. of Colloid and Interface Sci., 73 (1980) 212-223.
8. Truong, J.G. and Wayner, Jr., P.C., J. Chem. Phys., 87, (1987) 4180-4188.
9. DasGupta, S., Schonberg, J. A., Kim., I., Y., and Wayner, P. C. Jr., J. Colloid Interface Sci., 157 (1993) 332-342.
10. Wu, D. and Peterson, G. P., J. Thermophysics, 5 (1991) 129-134.
11. Khrustalev, D., and Faghri, A., Proceedings of National Heat Transfer Conference, Atlanta, GA 1993.
12. Swanson, L. W., and Peterson, G. P., Proceedings of the 1993 National Heat Transfer Conference, Atlanta, GA 1993.
13. Swanson and Herdt, J. Heat Transfer, 114 (1992) 434-441.
14. Wayner, Jr., P.C., Colloids and Surfaces, 52 (1991) 71-84.
15. DasGupta, S., Schonberg, J. A., and Wayner, P. C., Jr., J. Heat Transfer, 115 (1993) 201-208.
16. DasGupta, S., Sujanani, M., and Wayner, P.C., Jr., Proc. of the 2nd World Conference on Experimental Heat Transfer, Fluid Mechanics and Thermodynamics, Keffer, J. F. et al. ed., Elsevier Science Publishing Co. Inc., New York, 1991, pp. 361-368.
17. Gee, M.L., Healy, T.W., and White, L.R., J. Colloid Interface Sci., 131(1) (1989) 18-23.
18. Hough, D. B, and White, L. R., Adv. Colloid Interface Sci., 14 (1980) 3-41.
19. Dzyaloshinskii, I. E., Lifshitz, E. M., and Pitaevskii, L. P., Ad. Phys., 10 (1961) 165-209.
20. Blake, T. D., J. Chem. Soc., Faraday Trans. 1, 71 (1975) 192-208.
21. Beaglehole, D., Radlinska, E. Z., Ninham, B. W., and H. K. Christenson, Phys. Rev. Lett., 66(16) (1991) 2084-2087.
22. Beaglehole, D., and H. K. Christenson, J. Phys. Chem., 96 (1992) 3395-3403.
23. Stephan, P.C. and Busse, C.A., Int. J. Heat Mass Transfer, 35 (1992) 383-391.
24. Schonberg, J. A., DasGupta, S., and Wayner, P. C., Aerospace Heat Exchanger Technology 1993, R. K. Shah and A. Hashemi (Eds.), Elsevier Science Publishers B. V., 1993 pp. 239-254.

C-4.

$$P_v = P_\ell + \sigma K + \frac{(-B)}{\delta^h}$$
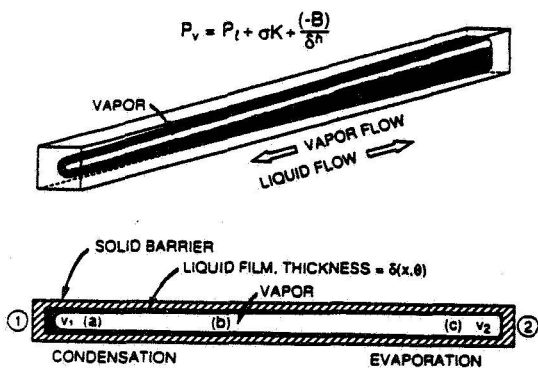
Fig. 1 CVBT Concept.

Fig. 2 Schematic Diagram of the Experimental Set-up.

90 μm

Fig. 3 Interference Fringes for Pentane on Quartz.

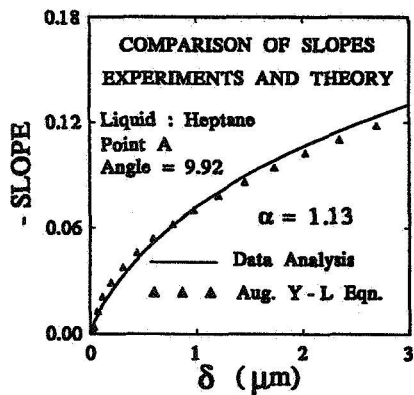Fig. 4 Film Thickness Profiles of Heptane at Different Positions for an Inclination Angle of 6.24°.

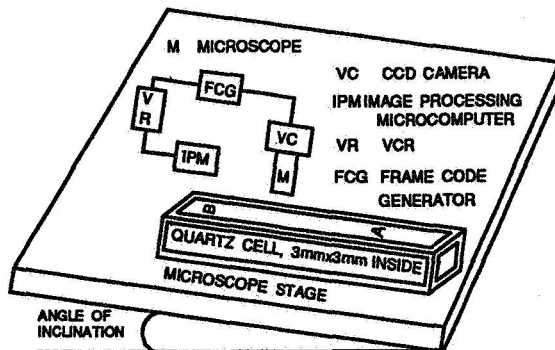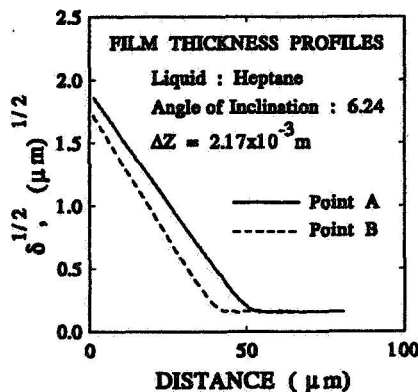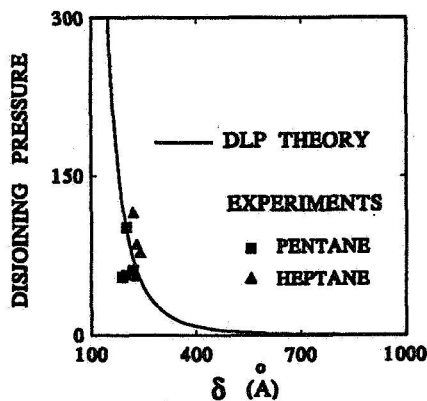Fig. 5 Comparison of the Experimental Slope and the slope from the Augmented Young-Laplace Equation (Eq. 11).

Fig. 6 Comparison of the Experiments and DLP Theory for the Adsorption of Pentane and Heptane on Quartz.